Interfacial propulsion by directional adhesion

Citation: Prakash, Manu, and John W.M. Bush. "Interfacial Propulsion by Directional Adhesion." International Journal of Non-Linear Mechanics 46, no. 4 (May 2011): 607–615.

As Published: http://dx.doi.org/10.1016/j.ijnonlinmec.2010.12.003

Publisher: Elsevier

Persistent URL: http://hdl.handle.net/1721.1/99431

Version: Author's final manuscript: final author's manuscript post peer review, without publisher's formatting or copy editing

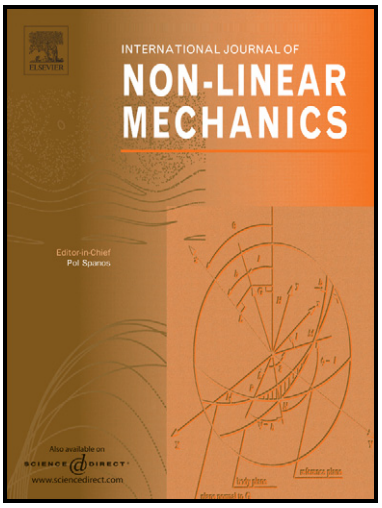

www.elsevier.com/locate/nlm

Interfacial propulsion by directional adhesion

Manu Prakash, John W.M. Bush

PII: S0020-7462(10)00183-6
DOI: doi:10.1016/j.ijnonlinmec.2010.12.003
Reference: NLM 1791

To appear in: *International Journal of Non-Linear Mechanics*

Received date: 16 March 2010
Revised date: 2 December 2010
Accepted date: 4 December 2010

Cite this article as: Manu Prakash and John W.M. Bush, Interfacial propulsion by directional adhesion, *International Journal of Non-Linear Mechanics*, doi:10.1016/j.ijnonlinmec.2010.12.003

Interfacial propulsion by directional adhesion

Manu Prakash[a,c], John W. M. Bush[b]

[a] *Junior Fellow, Harvard Society of Fellows, Harvard University*
[b] *Department of Mathematics, Massachusetts Institute of Technology*
[c] *Future home: Department of Bioengineering, Stanford University*

Abstract

The rough integument of water-walking arthropods is well known to be responsible for their water-repellency [1, 2, 3, 4]; however, water-repellent surfaces generally experience reduced traction at an air-water interface [5, 6, 7, 8]. A conundrum then arises as to how such creatures generate significant propulsive forces while retaining their water-repellency. We here demonstrate through a series of experiments that they do so by virtue of the detailed form of their integument; specifically, their tilted, flexible hairs interact with the free surface to generate directionally anisotropic adhesive forces that facilitate locomotion. We thus provide new rationale for the fundamental topological difference in the roughness on plants and water-walking arthropods, and suggest new directions for the design and fabrication of unidirectional superhydrophobic surfaces.

Keywords: Unidirectional superhydrophobic surfaces, propulsion on interfaces, water strider, force spectroscopy on a fluid interface

1. Introduction

The water-proofing strategies of plants [9, 10] and insects [1, 11, 12] have provided important guidance in the development of superhydrophobic surfaces [13, 14, 15] that are finding myriad industrial applications owing to their ability to resist corrosion, reduce drag, control adhesion and self-clean [16, 5, 6, 7, 17]. The dynamics of water-walking insects and spiders have received considerable recent attention [18, 19, 20, 21], in part because it touches on the burgeoning field of water-repellency [13, 14, 15, 8].

The simplest way to rationalize the propulsion of water-walking arthropods is to note that they transfer momentum to the underlying fluid: con-

servation of momentum requires that they be propelled forward [22, 19, 23]. This physical picture is here augmented by an examination of the direct forces acting on the creature. While it is known that most water-walking arthropods rely predominantly on capillary forces for their propulsion [19], elucidating the precise nature of these forces requires consideration of the micron-scale interaction of the arthropod cuticle and air-water surface.

When a water droplet wets a flat solid, the angle between the wetted solid surface and the interface, the chemical contact angle θ_e, is prescribed in terms of the magnitudes of the surface energies of the interface and the wet and dry solids by Young's equation [24]. The solid is defined as hydrophilic or hydrophobic according to whether θ_e is, respectively, less than or greater than 90°, and superhydrophobic if $\theta_e > 150°$. In practice, a finite range of static contact angles may be observed [25, 26]: static contact angles may lie anywhere in a finite range bounded above and below by the values at which contact line motion is initiated, specifically, the advancing and receding contact angles. An important consequence of this so-called contact angle hysteresis is a contact force that causes droplets to adhere to surfaces; for example, rain drops may stick to window panes because of the difference in the contact angles on their upper and lower edges [27]. A water-repellent surface must not only exhibit a high contact angle, but have a sufficiently low contact force that impinging water droplets roll off rather than stick. Generating water-repellency generally requires the use of hydrophobic, roughened surfaces, the roughness increasing the energetic cost of wetting the solid and so discouraging fluid-solid contact [28]. When the surface is sufficiently rough, air is trapped in the inclusions, leading to a Cassie state [29] in which apparent contact angles are greatly increased, while contact angle hysteresis and the resulting contact forces are drastically diminished [30].

The leaves of the lotus flower and many other plants are water-repellent by virtue of their waxy, rough surface structure [9, 10]: hierarchical roughness often in the form of micron- and submicron-scale bumps preserves a Cassie state. The piliferous integument of water-walking arthropods, though topologically distinct, plays a similar role in maintaining water-repellency and so preventing the creatures from sinking through the free surface [1, 11, 12, 31]. Critically, its surface consists of a waxy substance that increases the chemical contact angle to approximately 105° [32]. While there is a wide variation between species and body parts, roughness on the legs typically takes the form of a coherent array of hairs of characteristic width 1-3μm, spacing $\delta \sim 5 - 10\mu$m and length 20-50μm (Figure 1), tilted in the direction of the

leg tips. The water strider has leg hairs tilted so as to lie roughly tangent to the leg surface (Figure 1), thereby enhancing the resistance to fluid impregnation [1]. Andersen [2] reported that the hairs of the water strider are decorated with longitudinal, fluted grooves now known to have characteristic width 400nm and depth 200nm [3] (Figure 1c,d). The importance of these grooves in increasing the apparent contact angle of the water strider to 167° has recently been identified [4]; however, the dynamical significance of the linear roughness, specifically the hair and nanogroove topology, has yet to be considered.

Water-walking arthropods must not only maintain their water-repellency, but propel themselves through their interaction with the interface. These two requirement are at odds owing to the drag-reducing characteristics of superhydrophobic surfaces: when a rough surface in a Cassie state advances through a fluid, the opposing viscous stresses may be substantially reduced owing to the air layer adjoining the solid [7, 8]. Nevertheless, these dual requirements may be achieved with anisotropic roughness [5, 6, 7]. Choi *et al.* [6] examined the fluid flow past a surface in a Cassie state sustained by microchannels of characteristic width and depth 200nm. Drag was found to be reduced and enhanced relative to that on a smooth surface for flow directions respectively parallel and perpendicular to the grating. Yoshimitsu *et al.* [33] examined the force of adhesion that acts on water droplets suspended in a Cassie state on tilted surfaces decorated with grooves of characteristic width 50 μm. Drops rolled with greatest ease in the direction of the grooves and with greatest difficulty perpendicular to them. We here demonstrate that the tilted, grooved topology of the hairs of water-walking arthropods similarly serves to reduce the drag on legs gliding along their length, while increasing the resistance to leg motion perpendicular to the direction of motion.

New microscopic imaging of the interaction of arthropod cuticle and the water surface reveals that the principle propulsive forces correspond to contact forces acting through individual hairs on the driving legs. Direct force measurements reveal that the piliferous surface renders these adhesive forces directionally anisotropic: by virtue of the coherent tilted hair geometry, the force resisting relative motion between the fluid and cuticle is greatest for motion perpendicular to the leg. We report that the individual hairs bend in response to the capillary forces applied by the free surface, thus rendering the cuticle unidirectional: fluid glides with greatest ease towards the leg tips. Our new measurements of unidirectional adhesion on the cuticle make clear its critical dynamic role, yielding new insight into the manner in which

water-walking arthropods generate thrust, detach from and glide along the free surface.

2. Experimental study

All insects were captured at Fresh Pond in Cambridge MA, maintained in laboratory aquariums during the course of the experiments, and sustained by a regular diet of terrestrial insects. The integument of several water-walking arthropods was examined using a scanning electron microscope (XL30 ESEM) at various magnifications. Figure 1 illustrates an adult water strider *Gerris remigis*, and close-ups of its driving leg. No treatment was applied prior to SEM imaging. Note the linear roughness characteristic of water-walking insect cuticle [2, 3].

2.1. Observation of the Cassie state

Live *Microvelia* and adult water striders were imaged using a bright field microscope (LSM Pascal 5, Zeiss Confocal microscope) with an inverted stage. Insects moved freely on a water surface contained within a sample vial with its bottom surface replaced by a transparent cover slip of thickness 1mm. Images were captured when the insects entered the microscopes field of view. Figure 2a shows a live *Microvelia* in the process of grooming while standing on a fluid interface. The images were captured at various magnifications using an AxioCam HRM monochromatic camera from Zeiss. The field of view was sufficiently distant from the sidewall to avoid distortion by the menisci and thus ensure a flat focal plane.

In order for water-walking arthropods to remain water-repellent, a Cassie state must be maintained in both static and dynamic settings. Figure 2 provides clear photographic evidence that the cuticle of both *Microvelia* and the water strider are in Cassie states as they move freely on the water surface: the contact between the insects and water arises exclusively through the individual hairs and an air layer is trapped between the insect leg and water surface (Figure 3). Maintenance of the Cassie state on a solid with roughness of characteristic scale δ requires that the fluid pressure not exceed the curvature pressures σ/δ generated as the fluid tries to impregnate the rough solid (where σ is the surface tension) [34, 35]. Balancing this curvature pressure with the dynamic pressure, ρU^2, generated by the driving stroke or raindrop impact yields a wetting speed $U_w \sim (\sigma/\rho\delta)^{1/2} \sim 2$ m/s for the geometry

of strider cuticle evident in Figure 1, where $\delta \sim 10\mu$m is the characteristic spacing between hairs and ρ is density.

To examine the dynamic wettability of the strider integument, six tarsal leg segments, 0.5cm in length, were freshly cut from the rowing (middle) legs of four different recently deceased adult water striders and mounted on a 100μm steel pins using a quick-curing two-part epoxy (Hardman). Care was taken not to contaminate the samples during mounting. The samples were stored in a clean sealed container at room temperature for the duration of the experiments and used the same day that they were cut and mounted. If wetted during the course of an experiment, the integument would dry at room temperature via evaporation in less than 5 minutes.

The leg segments were mounted horizontally on a Newport micrometer stage. Spherical water droplets ranging in diameter from 50 to 200 µm were generated from the breakup of a water jet expelled from a tapered capillary. 20 experiments involving over 200 impacts were performed on three different adult water strider legs. At low speeds, the drops bounced off the leg without wetting it. At higher speeds, the collision left a microdroplet on the leg, an indicator of a wetting event (Figure 4ab). Wetting speeds ranging from 100-300 cm/s were observed to depend on the droplet size, location and geometry of impact, and the age and cleanliness of the sample. (See Supplementary Videos 1ab). We note that the observed wetting speeds exceed the peak leg speed of the adult water strider (approximately 70 cm/s), but may be exceeded by the speed of incident raindrops, which thus pose the greatest danger to water-walking arthropods in terms of wetting.

2.2. Observations of directional anisotropy

Unidirectional adhesion on the driving leg of the water strider can be surmised directly by examining the leg's interaction with a water droplet under a high magnification microscope (Figure 5). As the droplet was brushed against the leg, a Cassie state was maintained. In interpreting Figure 5, it is important to note that droplet deformation reflects an increase in surface energy; therefore, motions generating the largest deformations are the most strongly resisted. For example, the severe drop distortions generated by motion perpendicular to the leg (Figure 5a) indicate large adhesive forces. Consistent with Yoshimitsu *et al.*'s [33] observations of directional adhesion on a nanograting, the surface distortions indicate that the drop translates with greatest ease parallel rather than perpendicular to the leg. Moreover,

the drop advances more easily towards the leg tip than in the opposite direction owing to the flexibility of the tilted hairs. When the drop moves towards the leg tip (with the grain), the hairs and interface are largely undeformed by their relative motion (Figure 5b). Conversely, when it moves against the grain, the droplet interface is strongly distorted (Figure 5c) and advances by a series of discrete depinning events from sharply bent hairs (Figure 5d). Following depinning, the interface retracts and the hairs snap back into position.

In order to characterize the degree of bending observed in the experiments, here we look at scaling relations for capillary forces inducing bending in the elastic individual hairs of the cuticle. Considering the balance between resisting elastic forces and bending capillary forces for a circular cross-section beam that is bent as an arc of a circle: $G \sim [EI/R_cL]/[2\pi r\sigma]$, where E is the Elastic modulus, I is bending moment, L is total length of the beam, R_c is bending radius (we assume $R_c \sim L$), r is radius of the beam and σ is the surface tension. Further simplification leads $G \sim 1/8[Er^3/\sigma]/L^2 \sim 1/8L_E^2/L^2$, where $L_E = \sqrt{Er^3/\sigma}$ is the elasto-capillary length [36, 37]. Plugging in characteristic numbers ($L \sim 30\mu m$, $r \sim 1/2\mu m$, $E \sim 10^{11} dynes/cm^2$) we obtain $G \sim 2.5$ which indicates that individual hairs will not show large deformations of the order of the length of the hair (where $R_c \sim L$) when pulled by capillary forces grabbing the tip of the hair. However owing to very strong dependence on r, we note that G characterizing these tapered hair geometries found in the insect cuticle can be significantly less than 1. This simple scaling is consistent with our observations that hair deformation is largely confined to the tip regions (Figure 5d).

To further characterize and predict the actual deflections observed in experiments, we do an energy balance between elastic and capillary forces to calculate the predicted bending, again for a circular beam. The bending energy stored in a circular beam is $E_b \sim Er^4L/R_c^2$, where E is the elastic modulus, r is radius of the beam, L is total length and R_c is the effective bend radius. The surface energy gained by the contact surface $E_s \sim \sigma S \sim \sigma\pi r L_1$ where σ is the surface tension and L_1 is contact length along the side of the hair ($L_1 < L$, where L_1 part of the hair immersed in the fluid). From the two we obtain, $R \sim \sqrt{[(Er^3L)/(\pi\sigma L_1)]} \sim L_E\sqrt{[L/L_1)]}$ where L_E is the elasto-capillary length. The total tip deflection can be calculated from the length of the chord of a circle of radius R and arc length L given by $\delta = R(1-cos(L/R))$. Plugging the appropriate numbers, we obtain $\delta \sim 2\mu m$ which is close to our experimental observations of tip deflection of $2-5\mu m$

for hair in the insect cuticle .

Here we describe some simple observations that also support the idea of directional anisotropy, which we confirm in §2.3 with direct measurement. A recently deceased strider was placed on the free surface and subjected to a steady wind. Instead of turning perpendicular to the wind as does a floating canoe, the inanimate strider turns to glide in the direction of the wind (Figure 6) independent of the original orientation of the insect. The response of live striders to high wind also reflects their exploitation of directional adhesion: they assume a characteristic posture with their longest pair of driving legs extended perpendicular to the incident wind and lowered to the water surface in order to maximize their resistance to gliding. We note that the inference of directional anisotropy is consistent with the behaviour of water striders on rapidly flowing streams: when facing upstream, they remain stationary with very little effort, but when facing downstream, they are rapidly swept in that direction. This series of observations motivated a detailed study of interaction of insect cuticle with fluid interfaces.

2.3. Direct force measurements confirm directional anisotropy

Six tarsal segments were used in our measurements of contact forces and video microscopy of the cuticle deflection. Direct measurements of forces generated by brushing water droplets with insect integument were made using a dArsonval Galvanometer (Simpson Electric Co. SK525-457-4) (Figure 7), similar to a micro-force measurement apparatus of Livesay and Belser [38] that yielded a resolution of 0.05 dynes. Tarsal leg segments were mounted on the Galvanometer needle, along with a 2mm by 2mm platinum-coated silicon mirror. The deflection of a He-Ne red laser (Melles-Griot) beam from the mirror was recorded by a quad cell photo-detector (SPOT- 9DMI, UDT Inc.) after passing through a beam splitter. A low-noise voltage pre-amplifier (SR 560, Gain 200) was used to amplify the signal and control the input current in the Galvanometer coil. The torque supplied by the Galvanometer coil exactly balances the dynamic torque applied by the water droplet on the leg segment. The current in the Galvanometer coil, recorded via an A/D convertor (1kHz sampling rate, LabView software) and analyzed using Matlab software, is proportional to and so yields the force applied on the leg sample. The entire instrument is isolated from vibrations and is enclosed in a sealed plexiglass container to avoid air drafts.

Water droplets 2 mm in diameter were supported by a 23 gauge blunt needle mounted on a computer-controlled linear actuator (Newport 850G)

and translated above the leg segment at a fixed speed between 0.2 mm/sec and 1 mm/sec in directions parallel and perpendicular to the leg segment (see Figure 5, Supplementary Videos 2 and 3). Calibration tests were conducted using a pre-calibrated force transducer GSO-10 (Transducer Techniques Inc.) with a force resolution of 5 dynes. Fifteen data sets were recorded in total. A high-speed video camera (Phantom V5.0, 1000 fps) recorded the translation sequence. Care was taken to ensure that the leg remained in a Cassie state at all times, as was evident by virtue of an air-film between the leg and droplet.

The distance between the leg segment and the suspended droplet was precisely controlled with a piezo-based motorized micrometer (Picomotor 8301, Newfocus) with a positioning accuracy of 100nm. Varying the distance of the droplet from the leg segment allowed us to measure the dependence of the contact forces on the penetration depth of the hair tips. Figure 8cd illustrates measurements from multiple runs on the same leg segment. Contact forces increased monotonically with penetration depth, indicating that water-walking arthropods may increase their propulsive force by pushing down on the interface during their driving stroke.

Figure 8a illustrates the force experienced by the driving leg as it is brushes past the droplet in directions parallel and perpendicular to its length at a uniform speed of 1 mm/s and penetration depth $h = 10\mu$m. The discrete jumps in the contact forces apparent for motion parallel to the leg are associated with the depinning of the droplet surface from individual hairs. The anisotropy of the integument was always apparent, regardless of penetration depth, with the adhesive forces for drop motion with the grain, against the grain and perpendicular to the leg typically varying in the proportions 1 to 2 to 4. The maximum contact force is that perpendicular to the driving leg, whose magnitude is bounded by the product of the surface tension and the perimeter of the wetted leg region. Integrating around the contact area of the water strider's driving legs suggests a total propulsive force of order 140 dynes that is roughly consistent with inferences based on rough scaling arguments [22, 19] and direct in vivo measurements [20].

The rowing stroke of an adult water strider (Supplementary Video 4) was recorded using an inverted microscope (Zeiss STEMI 2000) coupled to a high-speed video camera (Phantom V5.0, 3000 fps). The freely moving strider was confined to a small water surface (5 cm by 5 cm) in order to increase the chances of capturing its motion in the field of view. Figure 9 illustrates the driving stroke of the driving leg. The bright spot corresponds to the meniscus that marks the point of detachment of the leg from the interface.

Following the power stroke, the driving leg is extracted along its length in a peeling motion. This is great energy saving mechanism for the leg to be primed for next stroke. Though Kim et al [17] describe the energy saving due to presence of a superhydrophobic coating, peeling has never been observed before during the propulsion strokes. Our direct measurements indicate that the force required to extract a leg along its length is less than 1.0 dyne (Figure 8).

2.4. Fabrication of a unidirectional superhydrophobic surface by pattern peeling

We proceed by presenting a new approach to fabrication of artificial unidirectional superhydrophobic surfaces exploiting the mechanics of peeling. The technique relies on capillary bridges to form and break between two polymer films, thus allowing microscopic pillars with controlled directionality to be formed on very large surfaces. The process is also suitable for implementation in a roll-to-roll process for producing large sheets in a manufacturing setting. A peeling-based technique for fabrication of superhydrophobic surfaces was also recently proposed [39]; however our technique allows for control of pillar tilt, thus enabling large scale fabrication of unidirectional superhydrophobic surfaces.

To overcome the difficulties of three-dimensional fabrication techniques, we utilize the dynamics of peeling thin plastic sheets on patterned substrates for synthesizing anisotropic superhydrophobic surfaces. The process involves peeling a thin polyester based thermoplastic adhesive sheet (heated to its softening temperature) in a controlled manner over a fixed patterned substrate (a bed of close-packed polystyrene beads). Polystyerene beads (with diameter 20 to 100 microns) were attached to a glass plate with an epoxy adhesive in a random pattern. The thermoplastic sheet (BEMIS 5250, 75 microns thick) was attached to a flexible substrate (Kapton film, 100 microns thick) and mounted on a metal roller (5 cm diameter). The system was heated to 125°C and contact between sheet and beads was established. The roller was translated by a motorized stage at a set velocity of 5 mm/sec. The net diameter of the roller governs the tilt angle of the artificial hairs formed on the surface. The contact of each bead with the sheet results in a capillary bridge. Figure 10 depicts the resulting patterned substrate. This Pattern Peeling method requires no clean room or lithographic facilities and so can be readily scaled up to a roll-to-roll manufacturing process.

As shown in Figure 10, SEM imaging of the surface confirms the tilt of the projecting pillars. The surface was vapor silanized to ensure chemical contact angles greater than 90 degrees. A droplet on the same material with and without structural patterning of the surface is depicted for comparison (Figure 10 d,e). We are currently in the process of producing larger surfaces, with a view to enabling a new series of experiments aimed at characterizing the dynamic behaviour of this surface. These experiments will include studies of droplet bouncing, and the effects of random vibrations on drops placed on the unidirectional surface.

3. Discussion

When considered in light of recent advances in surface science, our observations lead us to a number of new conclusions concerning the dynamics of water-walking arthropods. It has long been understood that the characteristic hairy, waxy cuticle of water-walking insects and spiders renders them water-repellent. It was recently pointed out that the hierarchical linear structure of roughness of the water strider (Figure 1) is responsible for the high static contact angle [3]; however, its critical dynamic role has not previously been appreciated. We first demonstrated that, consistent with recent advances in surface science [33], by virtue of the tilt of the leg hairs, the integument is directionally anisotropic: fluid moves with greater ease parallel rather than perpendicular to the leg. Second, we provided the first experimental evidence that the leg hairs deform under the influence of capillary forces, thereby rendering the cuticle unidirectional: fluid moves with greatest ease towards the leg tips (Figure 5 and 8). Our observations of its unidirectionality reveal that the cuticle plays a key propulsive role in maximizing thrust during the driving stroke, minimizing the force of extraction (Figure 9) and minimizing drag during the gliding phase (Figure 6 and 8). Finally, direct measurements of adhesive forces on the driving leg of a water strider suggest propulsive forces consistent with those measured on live water striders by previous investigators [20]

Our observations of the unidirectional adhesive properties of arthropod integument also yield novel insight into the geometry of the driving stroke of water-walking arthropods. For example, the fisher spider [18] and water strider [2, 22] row, striking or brushing the surface with their driving legs tangent to the surface and perpendicular to the direction of motion: the resulting contact forces are thus maximized by both the orientation and grooved topol-

ogy of the hairs. In order to extract their legs from the free surface following the driving stroke, they withdraw them along their length through a peeling motion (see Figure 9, Supplementary Video 4). The grooves on the hairs thus serve both to increase thrust during the driving stroke, and to decrease the force of extraction. Moreover, by aligning their rear legs with the direction of motion and lifting their front pair of legs off the free surface during the driving stroke, they minimize their resistance to forward motion. Our study sets the stage for a more extensive examination of the correlation between the cuticle topology and propulsive efficiency of water-walking arthropods.

Our observations provide the first direct evidence of the flexibility of water-walking insect cuticle (Figure 5d) and its critical importance for interfacial propulsion. The contact forces generated by the driving stroke, as enhanced by the anisotropy of the insect cuticle in conjunction with the stroke geometry, provide the basis for the propulsion of water-walking arthropods. The emergent physical picture of the most specialized water-walking arthropods is thus only partially consistent with the nickname of their most common representative, the water strider or 'pond skater'. Their tarsi remain in the Cassie state and, by virtue of the tilted hair geometry, act as the blades on a skate: when the legs strike the surface perpendicular to their direction of motion, they optimally generate thrust through contact forces. When the legs are aligned with the direction of motion, they experience reduced drag and glide readily along the free surface. However, the unidirectional adhesion makes the legs more like traditional cross-country skis than skates, with the flexible, tilted hairs serving as a natural herringbone. The grooved hairs thus serve not only to increase the static contact angle on arthropod cuticle [3, 4] but play a key propulsive role in maximizing thrust during the driving stroke, minimizing the force of leg extraction, and minimizing drag during the gliding phase.

Despite a number of interesting exceptions (e.g. the rice plant [16]), plant leaves are generally characterized by isotropic roughness [9, 10]. Conversely, the leg cuticle of most water-walking insects is distinctly anisotropic, characterized by grooved hairs pointing towards the leg tips. This distinct form of roughness enables the integument to play the dual role of retaining water-repellency while enhancing propulsive forces at the interface. Our study makes clear why plants are bumpy and insects are hairy: as well as staying water-proof, insects must propel themselves along the water surface.

Finally, inspired by arthropod cuticle, we have produced analogous synthetic unidirectional superhydrophobic surfaces using the pattern peeling fab-

rication technique detailed in Figure 10. A tilted array of flexible posts ensures that drops can only advance in the direction the posts are pointing, for example, when the substrate is subjected to random oscillations. Such surfaces are likely to find application in dynamic water-repellency and directed fluid transport in microfluidic systems[40].

References

[1] D. J. Crisp, W. H. Thorpe, The water-protecting properties of insect hairs, Disc. Faraday Soc. 3 (1948) 210–220.

[2] N. M. Andersen, The Semiaquatic Bugs (Hemiptera, Gerromorpha): Phylogeny, Adaptations, Biogeography and Classification, Scandinavian Science Press Ltd., Klampenborg, Denmark, 1982.

[3] X. Gao, L. Jiang, Water-repellent legs of water striders, Nature 432 (2004) 36.

[4] X.-Q. Feng, X. Gao, Z. Wu, L. Jiang, Q.-S. Zheng, Superior water repellency of water strider legs with hierarchical structures: Experiments and analysis, Langmuir 23 (2007) 4892–4896.

[5] J. Ou, B. Perot, J. P. Rothstein, Laminar drag reduction in microchannels using ultrahydrophobic surfaces, Phys. Fluids 16, (2004) 4635–4643.

[6] C.-H. Choi, U. Ulmanella, J. Kim, C.-M. Ho, C.-J. Kim, Effective slip and friction reduction in nanograted superhydrophobic microchannels, Phys. Fluids 18 (2006) 087105.

[7] P. Joseph, C. Cottin-Bizonne, J. M. Benoît, C. Ybert, C. Journet, P. Tabeling, L. Bocquet, Slippage of water past superhydrophobic carbon nanotube forests in microchannels, Phys. Rev. Lett. 97 (2006) 156104.

[8] J. P. Rothstein, Slip on superhydrophobic surfaces, Annual Review of Fluid Mechanics 42 (2010) 89–109.

[9] P. Wagner, R. Furstner, W. Barthlott, C. Neinhuis, Quantitative assessment to the structural basis of water repellency in natural and technical surfaces, J. Exp. Bot. 54 (2003) 1295–1303.

[10] A. Otten, S. Herminghaus, How plants keep dry: A physicist's point of view, Langmuir 20 (2004) 2405–2408.

[11] P. Wagner, C. Neinhuis, W. Barthlott, Wettability and contaminability of insect wings as a function of their surface sculpture, Acta Zool. 77 (1996) 213–225.

[12] Y. Zheng, X. Gao, L. Jiang, Directional adhesion of superhydrophobic butterfly wings, Soft Mater. 3 (2007) 178–182.

[13] R. Furstner, W. Barthlott, C. Neinhuis, P. Walzel, Wetting and self-cleaning properties of artificial superhydrophobic surfaces, Langmuir 21 (2005) 956–961.

[14] X. Wu, G. Shi, Production and characterization of stable superhydrophobic surfaces based on copper hydroxide nanoneedles mimicking the legs of water striders, J. Phys. Chem. B 110 (2006) 11247–11252.

[15] X.-Q. Feng, L. Jiang, Design and creation of superwetting/antiwetting surfaces, Adv. Mater. 18 (2006) 3063–3078.

[16] X. Feng, S. Li, Y. Li, H. Li, L. Zhang, J. Zhai, Y. Song, B. Liu, L. Jiang, D. Zhu, Super-hydrophobic surfaces: From natural to artificial, Adv. Mater. 14 (2002) 1857 – 1860.

[17] D.-G. Lee, H.-Y. Kim, The role of superhydrophobicity in the adhesion of a floating cylinder, Journal of Fluid Mechanics 624 (2009) 23–32.

[18] R. B. Suter, R. B. Rosenberg, S. Loeb, H. Wildman, J. Long, Locomotion on the water surface: Propulsive mechanisms of the fisher spider *Dolomedes triton*, J. Exp. Biol. 200 (1997) 2523–2538.

[19] J. W. M. Bush, D. L. Hu, Walking on water: Biolocomotion at the interface, Ann. Rev. Fluid Mech. 38 (2006) 339–369.

[20] P. Perez-Goodwyn, K. Fujisaki, Sexual conflicts, loss of flight, and fitness gains in locomotion of polymorphic water striders (*Gerridae*), Entomol. Exper. Applic. (2007).

[21] D. Vella, D.-G. Lee, H.-Y. Kim, The load supported by a small floating object, Langmuir 22 (2006) 5979–5981.

[22] D. L. Hu, B. Chan, J. W. M. Bush, The hydrodynamics of water strider locomotion, Nature 424 (2003) 663–666.

[23] D. Hu, J. W. Bush, Hydrodynamics of water walking arthropods, Journal of Fluid Mechanics 644 (2010) 5–33.

[24] T. Young, An essay on the cohesion of fluids, Phil. Trans. Roy. Soc. Lond. A 95 (1805) 65–87.

[25] R. H. Dettre, R. E. Johnson, Contact angle hysteresis II. Contact angle measurements on rough surfaces, in: F. M. Fowkes (Ed.), Contact Angle, Wettability, and Adhesion, volume 43 of *Adv. Chem. Ser.*, American Chemical Society, Washington, DC, 1964, pp. 136–144.

[26] R. E. Johnson, R. H. Dettre, Contact angle hysteresis I. Study of an idealized rough surface, in: F. M. Fowkes (Ed.), Contact Angle, Wettability, and Adhesion, volume 43 of *Adv. Chem. Ser.*, American Chemical Society, Washington, DC, 1964, pp. 112–135.

[27] E. B. Dussan, R. T. Chow, On the ability of drops or bubbles to stick to non-horizontal surfaces of solids, J. Fluid Mech. 137 (1983) 1–29.

[28] R. N. Wenzel, Resistance of solid surfaces to wetting by water, Ind. Eng. Chem. 28 (1936) 988–994.

[29] A. B. D. Cassie, S. Baxter, Wettability of porous surfaces, Trans. Faraday Soc. 40 (1944) 546–551.

[30] P. G. de Gennes, F. Brochard-Wyart, D. Quéré, Capillarity and Wetting Phenomena: Drops, Bubbles, Pearls and Waves, Springer-Verlag, Berlin, 2003.

[31] J. W. M. Bush, M. Prakash, D. L. Hu, The surface structure of water-walking arthropods: form and function, Adv. Insect Physiol. (2008).

[32] M. W. Holdgate, The wetting of insect cuticle by water, J. Exp. Biol. (1955) 591–617.

[33] Z. Yoshimitsu, A. Nakajima, T. Watanabe, K. Hashimoto, Effects of surface structure on the hydrophobicity and sliding behavior of water droplets, Langmuir 3 (2002) 5818–5822.

[34] M. Reyssat, A. Pépin, F. Marty, Y. Chen, , D. Quéré, Bouncing transitions in microtextured materials, Europhys. Lett. 74 (2006) 306–312.

[35] D. Bartolo, F. Bouamrirene, E. Verneuil, A. Beguin, P. Silberzan, S. Moulinet, Bouncing or sticky droplets: impalement transitions on superhydrophobic micropatterned surfaces, Europhys. Letters 74 (2006) 299–305.

[36] J. Bico, B. Roman, Elasto-capillarity: deforming an elastic structure with a liquid droplet, J. Phys.: Cond. Mat. 22 (2010) 493101.

[37] J. Bico, B. Roman, L. Moulin, A. Boudaoud, Elastocapillary coalescence in wet hair, Nature 432 (2004) 690.

[38] B. R. Livesay, R. B. Belser, Instrument for measuring small frictional forces, Tribology Transactions 12 (1969) 257–265.

[39] S.-H. Hsu, W. M. Sigmund, Artificial hairy surfaces with a nearly perfect hydrophobic response, Langmuir 26 (2010) 1504–1506.

[40] M. Prakash, N. Gershenfeld, Microfluidic bubble logic, Science 315 (2007) 832–835.

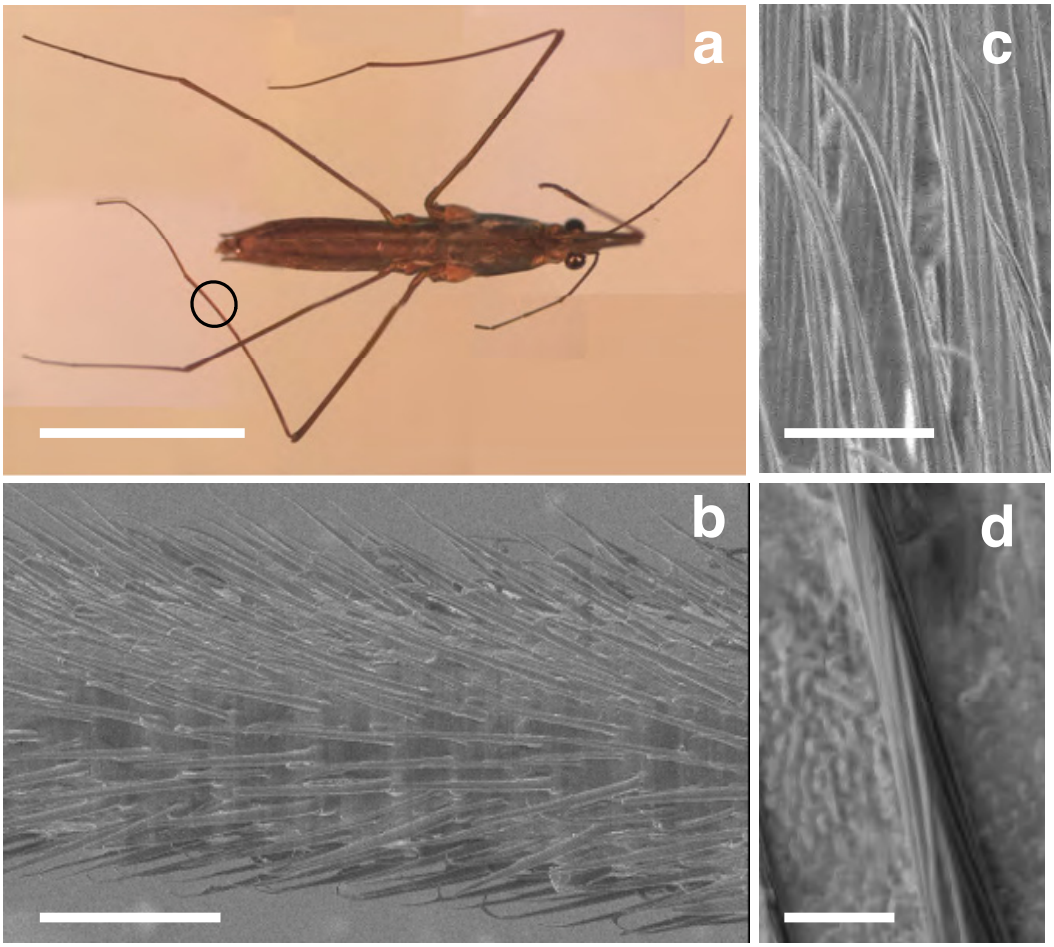

Figure 1: Scanning Electron Microscope (SEM) images of the rowing leg of the water strider (*Gerris remigis*). (**a**) The strider's legs are covered by an array of hairs tilted towards the leg tip. (**b**) The hairs have characteristic length 20 µm, radius 1 µm and are marked by longitudinal nanogrooves (**c, d**) roughly 400nm wide and 200nm deep [2, 3, 16]. Scale bars: **a)** 1 cm; **b)** 50 µm; **c)** 5 µm; **d)** 2.5 µm.

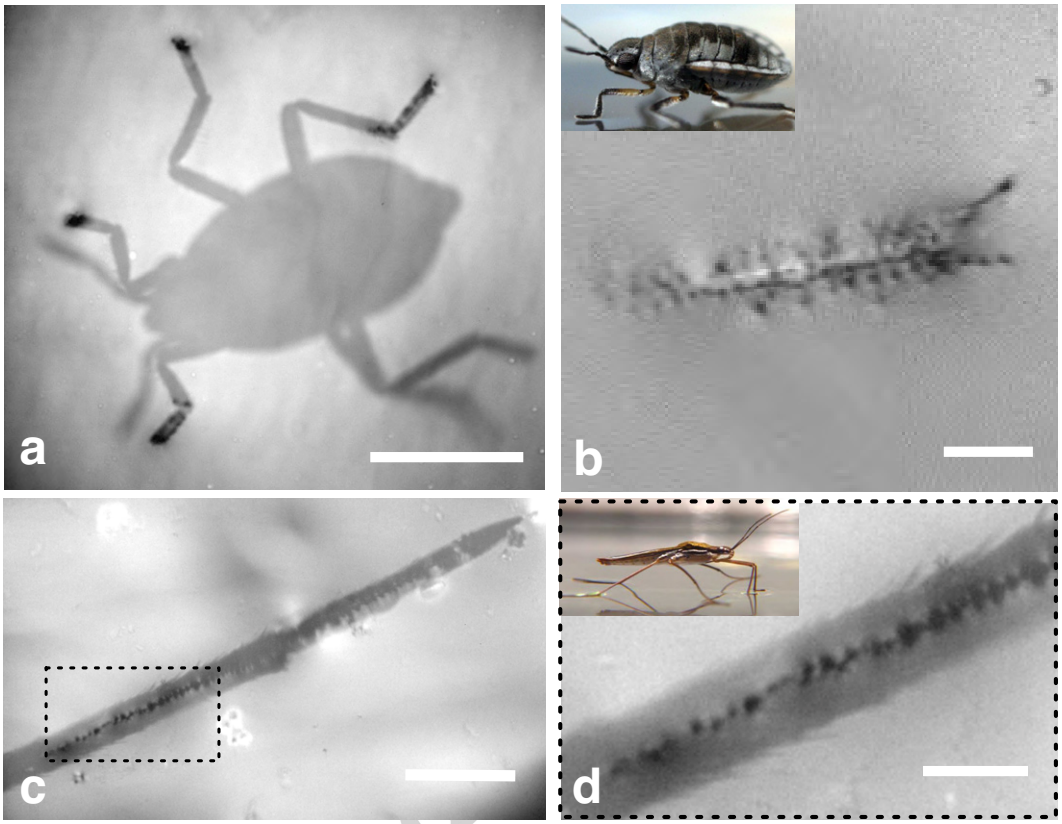

Figure 2: Brightfield microscope images of water-walking arthropods in a non-wetting Cassie state, captured with an inverted microscope (Zeiss LSM Pascal). **a**) A live *Microvelia* standing on the water surface grooming its water-repellent legs. **b**) A closer look at one of the supporting tarsi shows that contact between the cuticle and water surface arises exclusively through pin-holes (dark spots) associated with individual hairs. **c**) Contact line of the leg of a live water strider (*Gerris remigis*) standing on the water surface. **d**) Magnification of the marked region reveals that contact between insect and fluid arises exclusively through a single row of hairs. Scale bars: **a**) 1mm; **b**) 100 µm; **c**) 250 µm; **d**) 100 µm.

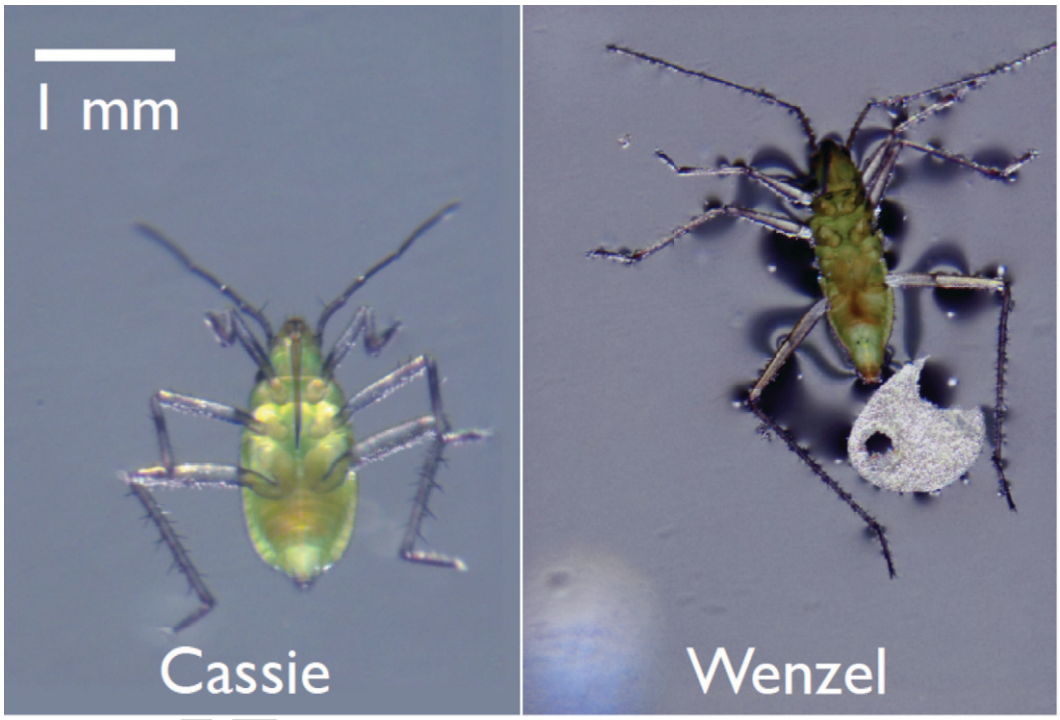

Figure 3: Inverted microscope images of a live *Microvelia* resting on the fluid interface in (a) Cassie and (b) Wenzel state. The former is its natural state, with contact only on its tarsae. The latter was forcibly wetted by emersion, giving rise to a contact line circumscribing the creature's legs, antennae and body cavity.

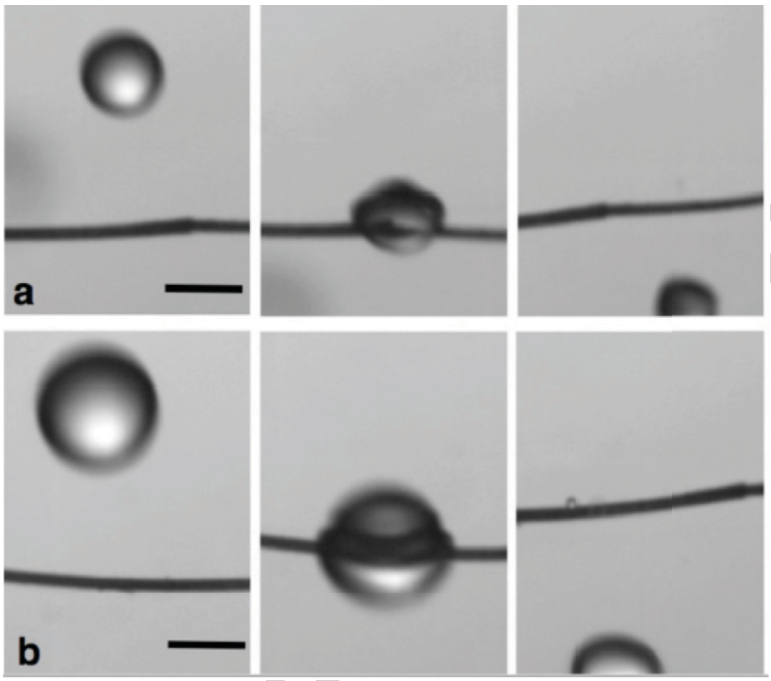

Figure 4: Impact of water droplets on a water strider leg. A critical velocity of impregnation of the hair layer exists for droplet impact. a) Below this wetting speed, droplets simply bounce off. b) Above it, small wetting drops in a Wenzel state are left behind. Scale bars, 1mm.

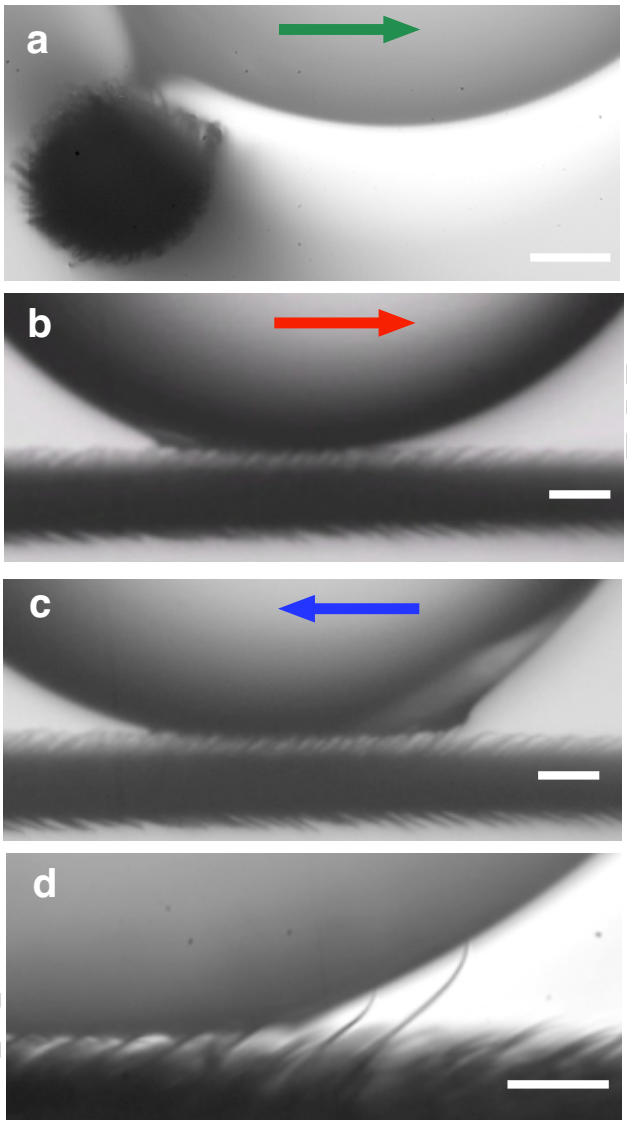

Figure 5: The interaction of insect cuticle with a translating water droplet. **a**) For drop motion perpendicular to the leg, severe drop deformations indicate large adhesive forces (also see Supplementary Videos 2,3). **b**) The drop moves with relative ease towards the leg tip, with little distortion of either hair or interface. **c**) For motion against the grain of the tilted hairs, the interface is snagged on the elastic hairs and drawn out into a thin sheet evident as a white triangle. **d**) Individual hairs are deflected by capillary forces as the drop advances against the grain.

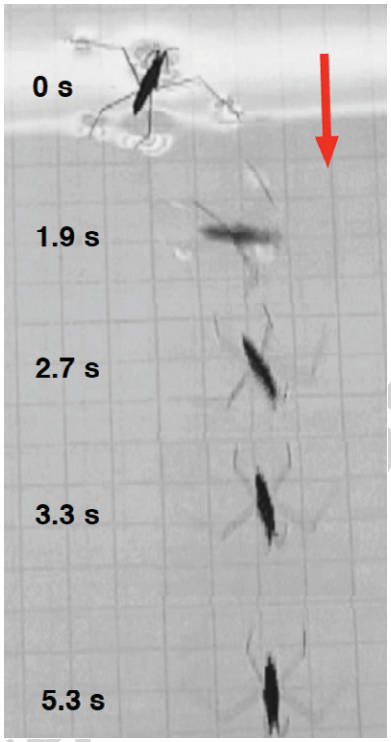

Figure 6: A recently deceased water strider responds to a gentle applied wind by turning to glide in the direction of least resistance, specifically downwind. The red arrows marks the direction of the wind. This realignment indicates the directional anisotropy of its cuticle.

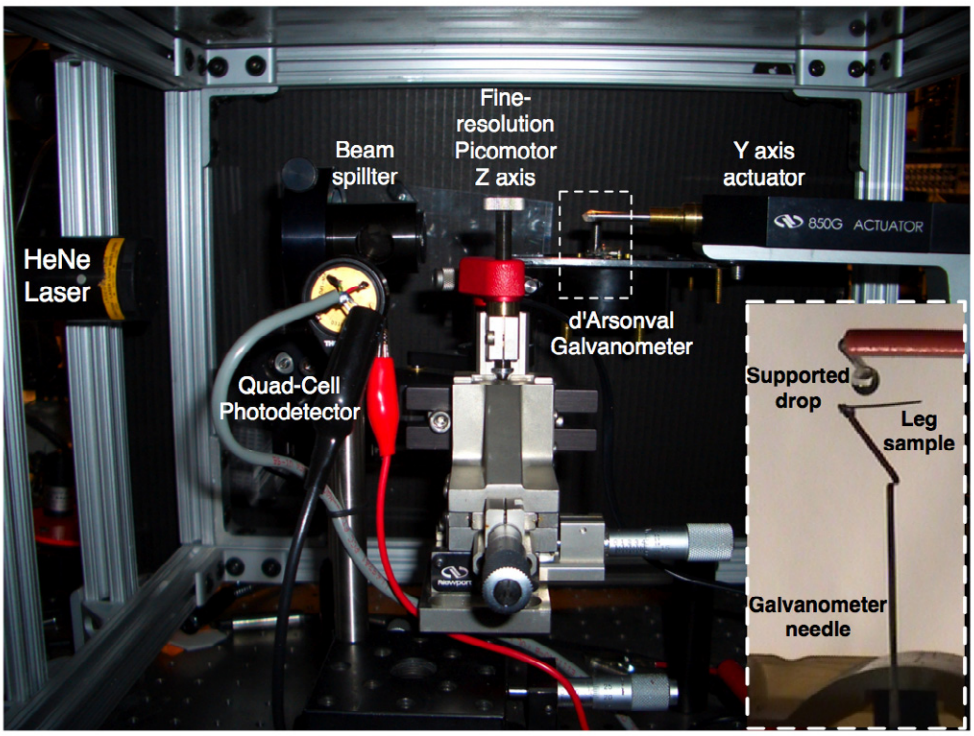

Figure 7: The experimental apparatus used for direct measurements of the resulting adhesive forces.A water strider leg is mounted on a spiral spring force balance. A hanging drop ($\sim$ 2mm diameter) is translated in the plane of the leg via a computer controlled Newport actuator. The force measurements were calibrated via a GSO-10 force transducer.

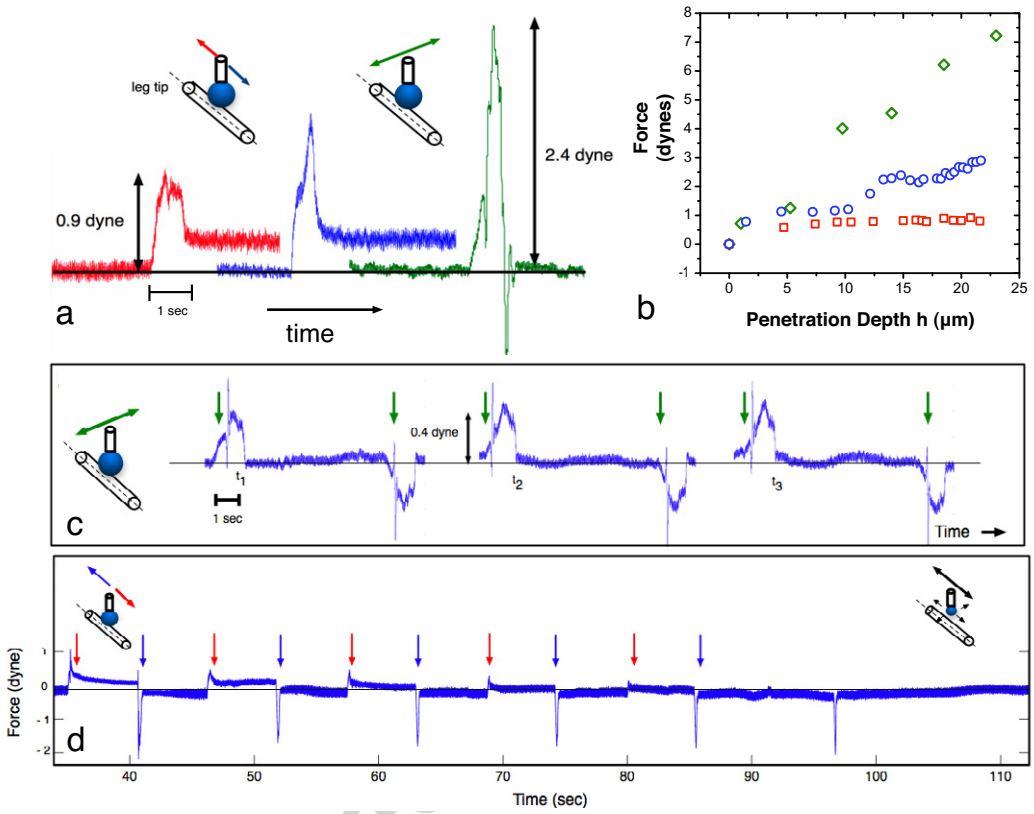

Figure 8: **a**) The evolution of the force per unit length on a water strider leg as the water droplet is translated past it in directions perpendicular to the leg (green), and parallel to the leg, both against (blue) and with (red) the grain. The mean penetration depth of the hair tips is $h = 10$ μm. **b**) The dependence of the three contact-force components on h. **c**) Three force-time curves measured as the drop is brushed by the leg moving in both directions perpendicular to its length demonstrate the repeatability of our experiments. The peaks correspond to periods of drop motion: the intervening at regions to a static setting. Depinning from an individual hair is evident as a pronounced spike in each of the three time series. **d**) The force-time curves generated as the drop is translated parallel to the leg surface both with (red) and against (blue) the grain. The peaks (highlighted by arrows) indicate contact forces generated by drop motion, while the relatively flat intervening regions correspond to residual forces arising during periods of stasis. Contact forces decrease steadily as the droplet evaporates and the penetration depth of the hair tips decreases. The directional anisotropy in the contact forces is again readily apparent.

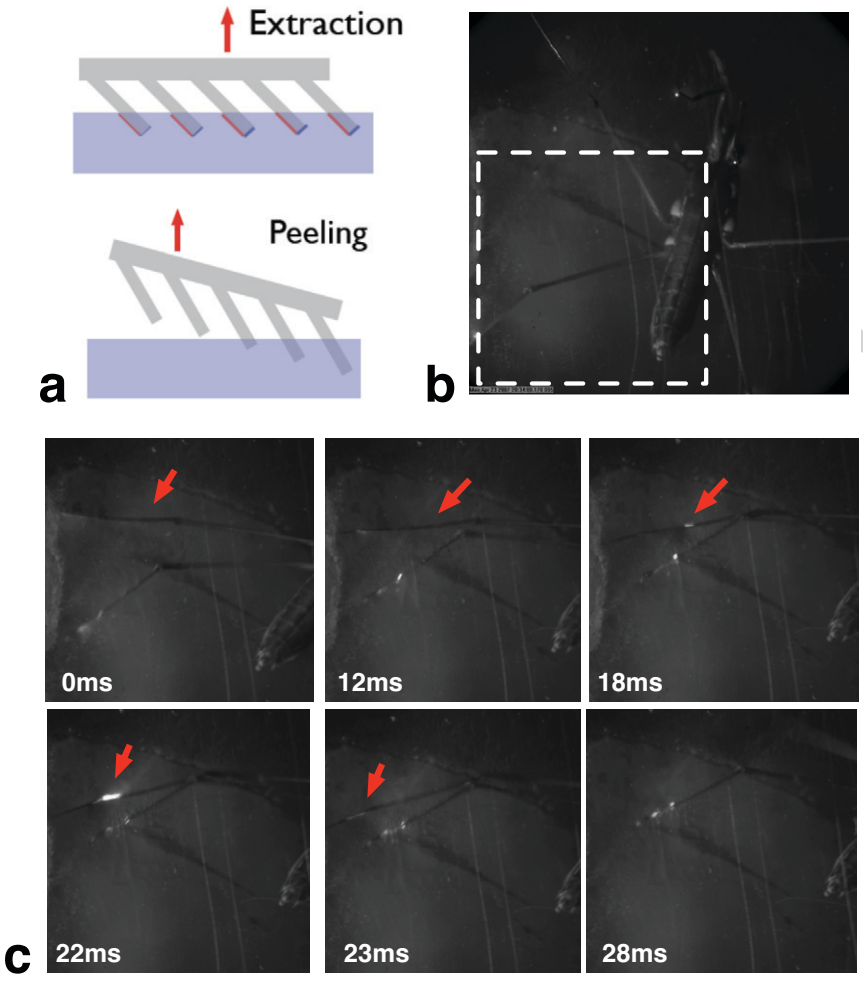

Figure 9: Inverted high-speed microscopy of the driving stroke and subsequent extraction of a water strider leg. The red arrow indicates the point beyond which the driving leg is in contact with the interface. The leg is withdrawn along its length in a peeling motion, thereby reducing the energetic cost of extraction.

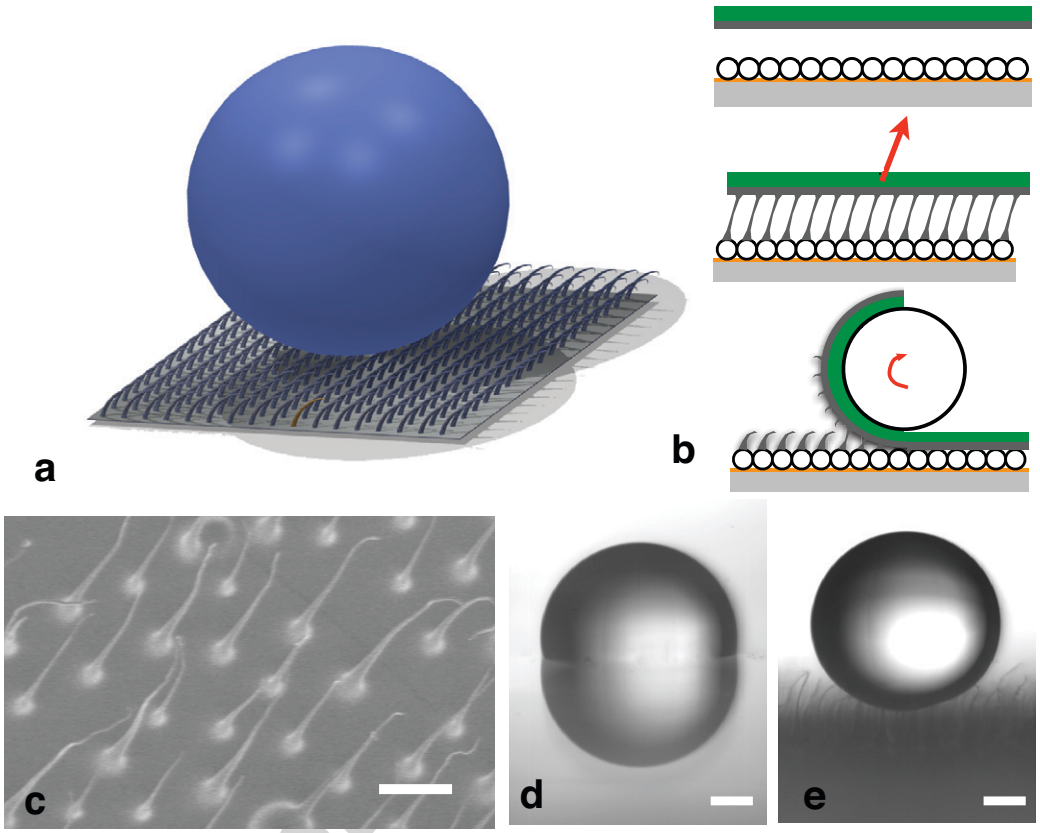

Figure 10: **a**) The 'Bug Rug': an idealized unidirectional superhydrophobic surface based on the form of water-walking arthropod cuticle. **b**) Schematic illustration of the pattern peeling technique used to fabricate such surfaces, for which no clean room or micro-fab facilities are required (see Supplementary Materials). **c**) SEM photomicrograph of a section of tilted pillars fabricated by peeling a polyester-based thermosetting adhesive film (BEMIS-5250, thickness 75 µm) off a bed of polystyrene beads (100 micron diameter, Polymicro). The resulting pillars are tilted at an average angle of 45 degrees. Water drops sitting on **d**) a flat sheet of the silanized polymer film and (**e**) the polymer film textured by pattern peeling. Scale bars **c**) 200 µm; **d**) 500 µm; **e**) 500 µm.